Traffic 2013; **14:** 487–501

doi:10.1111/tra.12048

Quantitative Analysis of Membrane Protein Transport Across the Nuclear Pore Complex

Anne C. Meinema[1], Bert Poolman[1] and Liesbeth M. Veenhoff[1,2,*]

[1]Department of Biochemistry, Groningen Biomolecular Sciences and Biotechnology Institute, Netherlands Proteomics Centre, Zernike Institute for Advanced Materials, University of Groningen, Nijenborgh 4, 9747 AG, Groningen, the Netherlands
[2]European Research Institute for the Biology of Ageing, University Medical Centre Groningen, University of Groningen, Groningen, the Netherlands

**Corresponding author: Liesbeth M. Veenhoff, l.m.veenhoff@rug.nl*

Nuclear transport of the *Saccharomyces cerevisiae* membrane proteins Src1/Heh1 and Heh2 across the NPC is facilitated by a long intrinsically disordered linker between the nuclear localization signal (NLS) and the transmembrane domain. The import of reporter proteins derived from Heh2 is dependent on the FG-Nups in the central channel, and the linker can position the transport factor-bound NLS in the vicinity of the FG-Nups in the central channel, while the transmembrane segment resides in the pore membrane. Here, we present a quantitative analysis of karyopherin-mediated import and passive efflux of reporter proteins derived from Heh2, including data on the mobility of the reporter proteins in different membrane compartments. We show that membrane proteins with extralumenal domains up to 174 kDa, terminal to the linker and NLS, passively leak out of the nucleus via the NPC, albeit at a slow rate. We propose that also during passive efflux, the unfolded linker facilitates the passage of extralumenal domains through the central channel of the NPC.

Key words: inner nuclear membrane, intrinsically disordered, membrane protein, nuclear envelope, nuclear pore complex, nuclear transport

Received 16 March 2012, revised and accepted for publication 22 January 2013, uncorrected manuscript published online 28 January 2013, published online 21 February 2013

Integral membrane proteins with a nuclear function can be transported via the nuclear pore complex (NPC). The outer nuclear membrane (ONM) is continuous with the inner nuclear membrane (INM) via the sharply curved pore membrane (POM), at sites where the NPCs are anchored in the nuclear envelope (NE) (1). Different mechanisms have been proposed for the traffic of these integral membrane proteins [reviewed by (2–6)]. Early publications supported a diffusion/retention model (7), in which membrane proteins traverse the NPC by diffusion (1,8,9) and accumulate at the INM by binding to nuclear structures (10–13). This diffusion across the NPC was thought to occur through the narrow lateral or peripheral channels along the POM (8,14,15). It has been reported that these ∼10 nm wide channels allows passage of molecules of up to ∼60 kDa (8,13).

While for most membrane proteins of the INM studied so far, nuclear retention is an important determinant for their localization, specific domains or signals that contribute to targeting to or across the NPCs have been reported in recent years (16–20). Indeed, some membrane proteins are imported through a mechanism that is reminiscent of that used by soluble proteins. Many soluble proteins that carry a nuclear localization signal (NLS) are chaperoned across the NPC by nuclear import factors belonging to the family of karyopherins (Kaps) [reviewed in (21)]. A basic classical NLS (cNLS), as a single partite or a bipartite sequence (22), for example, is recognized by the adapter proteins Kap-α (importin-α). For nuclear transport it additionally requires Kap-β1 (importin-β1), which interacts with the phenylalanine-glycine (FG)-repeats abundantly present in a subset of NPC proteins, the FG-nucleoporins. Once the Kap-cargo-complex reaches the nuclear side of the NPC, binding to nuclear localized RanGTP leads to dissociation of the cargo, whereby the Kaps are recycled back to the cytoplasm [reviewed in (23,24)]. The kinetics of facilitated import and passive leak (efflux) across the NPC, together with possible retention at either the nuclear or cytoplasmic compartment determine the localization of proteins. NLS sequences that attract the transport factors Kapβ via Kapα have been identified in several membrane proteins, including the human SUN2 (17), *Caenorhabditis elegans* Unc-84 (18), and the human Pom121 (19). The NLSs are not the only sequences that contribute to the targeting of these proteins. For example, Unc-84 has besides two cNLSs an INM sorting motif, consisting of three lysines at the cytoplasmic side of a transmembrane helix, and a conserved region called the SUN-nuclear envelop localization signal. SUN2 targeting relies on a functional cNLS, a Golgi retrieval signal and a luminal SUN domain to contribute to targeting to the INM.

The *Saccharomyces cerevisiae* proteins Src1/Heh1 and Heh2, homologous of the metazoan MAN1 and LEM2, have a bipartite NLS sequence that is bound by Kap60, the yeast homologue of Kap-α (16). The import of these proteins to the INM is dependent on the Kapβ homologue, Kap95, and the gradient of RanGTP across the NE (16). To further detail the Kap-mediated import mechanism, we designed reporter proteins based on Heh1 and Heh2 that had minimal features required for INM-targeting (20). Sufficient for efficient import to the INM are the high-affinity NLS of Heh2 (h2NLS) or Heh1 and a long intrinsically

disordered linker (L) between the NLS and the transmembrane domain. The disordered linker needs to be longer than 120 residues but no specific amino acid sequence is required. Also, synthetic transmembrane domains and polytopic membrane proteins are targeted to the INM if fused to an 'h2NLS-L' sequence. The import is dependent on the FG-Nups in the central channel, and we proposed that the linker is needed to position the Kap-bound NLS in the vicinity of the FG-Nups in the central channel, while the transmembrane segment(s) reside(s) in the pore membrane.

Retention also contributes to the localization of Heh2 at the INM as we see that upon blocking Kap-mediated transport, INM resident Heh2 stays at its location and only very slowly redistributes to the ER (20). In contrast, the Heh2-derived reporter proteins are mobile within the NE-ER network, and they redistribute over the NE-ER network after blocking Kap-mediated import. The reduced retention of the reporter proteins is likely because they lack the soluble N-terminal LEM (Lap2, Emerin, MAN1)-domain and the Man1-C-terminal homology domain that have binding partners at the inner nuclear membrane. In the current work, we make use of the mobility of the reporter proteins to obtain quantitative information on the kinetics of import and passive efflux across the NPC and the lateral diffusion of the reporter proteins in the different membrane compartments. We provide data to support that Kap60 (and Kap95) bind strongly to the h2NLS throughout the NE-ER network, effectively competing with the transport of soluble cargo. We compare import and efflux rates to those of soluble Kap60-cargo and conclude that import of membrane reporters is significantly slower than that of soluble reporters. We evaluate the transport of reporter proteins with large soluble domains of up to 174 kDa, which leave the INM compartments and travel back to the ONM and ER when Kap60/95 is eliminated. We discuss our findings in the light of the architecture of the NPC and the proposed transport path through the NPC central channel.

Results

Terminology

Our first goal is to determine the kinetics of nuclear import and efflux of membrane embedded reporter proteins in *Saccharomyces cerevisiae*, using the Heh2-based reporter protein GFP-h2NLS-L-TM [referred to as h2NLS-L-TM in (20)]. The movement of these membrane proteins to the INM involves both lateral diffusion to the NPC through the network of ER-ONM membranes and translocation across the NPC. We use the terms import (and export) for metabolic energy and Kap-dependent transport across the NPC. For equilibration and diffusion down the concentration gradient, i.e. transport independent of metabolic energy and Kaps, we use the terms passive influx and passive efflux. Mobility of proteins in the membrane is referred to as lateral diffusion and assumed to be 2D Brownian in nature.

We previously showed, using immunoEM, that the reporter protein GFP-h2NLS-L-TM is enriched at the inner nuclear membrane relative to the outer nuclear membrane and the peripheral ER (20). The enrichment of GFP-h2NLS-L-TM at the INM is observed in confocal images as increased fluorescence signal at the nuclear envelope compared to the peripheral ER, which we report as NE/ER ratio. For GFP-h2NLS-L-TM, the NE/ER-ratio was reproducibly found at 34.1 ± 4.9 (20) (Figure 1A,B). In the absence of functional Kap95, the accumulation is lost and a NE/ER-ratio of 2.2 ± 0.2 is measured (Figure 1B, +RAP). Reporter proteins with a shortened linker, GFP-h2NLS-L(37)-TM, or the reporter proteins without the h2NLS, GFP-L-TM, did not accumulate at the INM, and for these reporters we measured an NE/ER-ratio of 2.3 ± 0.2 and 2.3 ± 0.3 (20) (Figure 1A,B).

The expression levels of the membrane reporters are approximately equal and the concentration at the INM is thus highest for GFP-h2NLS-L-TM (20). The NE/ER-ratios are the experimental values that allow direct comparison of the accumulation levels at the INM of different cargos, or of the same cargo under different conditions. In addition, they can be interpreted as the resultant of import, influx and efflux across the NPC and diffusion through the membranes of the NE-ER network as indicated in Figure 1C. For movement towards the INM (k_{in}) we distinguish: lateral diffusion through the ER to the NPCs (k_1), and passive influx to the INM for proteins without an NLS (k_2) or active import facilitated by karyopherins (for proteins bearing an NLS) (k_3). For the outward pathway from the INM (k_{out}), we distinguish nuclear efflux to the ONM (k_{-2}) and lateral diffusion in the ONM/ER away from the NPCs (k_{-1}). We have no evidence for active export and therefore assume reporter proteins to leave the INM via passive efflux. The kinetics of Kap60 and Kap95 association and dissociation in the ER and ONM are not included as they not likely influence the overall import (and efflux), as shown in Figures 2 and 3. The measured efflux rate constants in Figures 6 and 7 thus reflect k_{-1} and k_{-2}, while the calculated overall import rate constant includes k_1, k_2 and k_3.

Transport factor binds h2NLS-reporter throughout the NE-ER network

A transport reaction starts with the recruitment of Kap60 and Kap95 onto the reporter protein. The h2NLS has high affinity compared to the cNLS or other bipartite NLSs (20,25,26). We examined whether the reporter proteins stably complex with Kap60 and Kap95 while in the NE-ER network. If an h2NLS-reporter is stably bound by Kap60 and Kap95, one expects Kap95-GFP to enrich at those membranes where the reporter resides. Normally, Kap95-GFP is present in the cytoplasm and accumulates at the NE, but one does not observe residence at the ER (Figure 2A) (27). We asked if we could see that

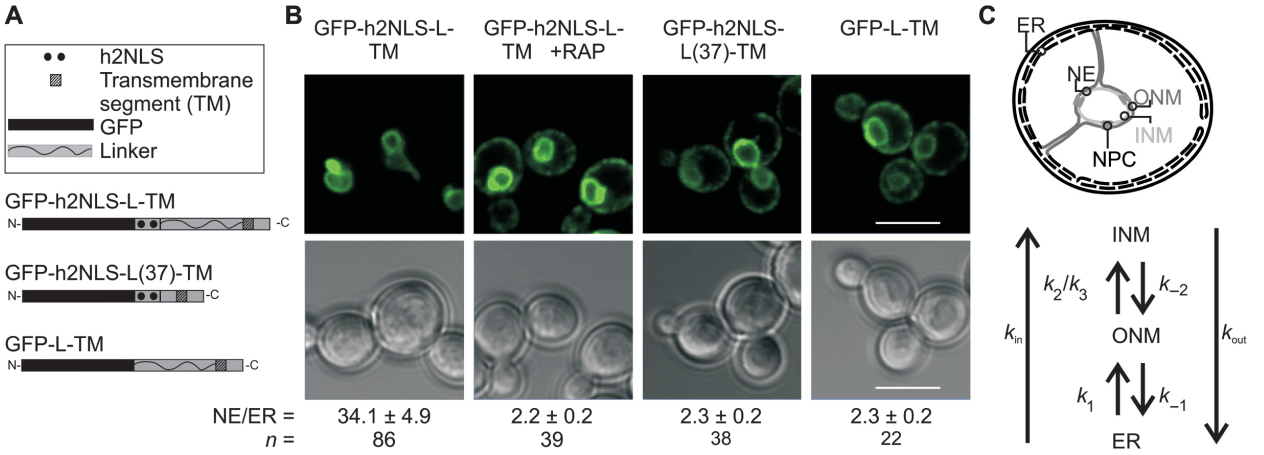

Figure 1: Import to the INM of Heh2-based reporter proteins. A) Cartoons indicate domain composition of the reporter proteins. B) Confocal images showing the localization of Heh2-derived reporter proteins; cartoons indicate domain composition of the reporter proteins. The GFP-h2NLS-L-TM reporter protein is efficiently imported to the INM resulting in increased fluorescence at the NE compared to the ER, while the GFP-h2NLS-L(37)-TM and GFP-L-TM reporter proteins are not, and show lower accumulation (20). In the presence of rapamycin (+Rap), cells are depleted of functional Kap95 and GFP-h2NLS-L-TM has approximately equal intensity at the NE and ER. Average NE/ER ratios, reflecting the average pixel intensity at the NE divided by that at the ER, over n cells are indicated below the images. C) For the overall flux of membrane proteins to the INM (k_{in}), we distinguish lateral diffusion through ER and ONM to the NPCs (k_1), diffusion across the NPC (influx) (k_2) or Kap-facilitated import (k_3). For the overall efflux (k_{out}), we distinguish diffusion across the NPC (efflux) (k_{-2}) and lateral diffusion from ONM to ER (k_{-1}). Scale bar is 5 μm.

Kap95 localized to the ER in cells with high levels of an h2NLS-containing reporter. As shown in Figure 1, the concentrations of the GFP-h2NLS-L(37)-TM reporter is high at the ER due to inefficient import. Indeed, when we co-expressed Kap95-GFP with the mCherry (mCh)-tagged reporter, mCh-h2NLS-L(37)-TM, we observed that in ∼80% of the cells where the mCh-reporter was visible at the peripheral ER, Kap95-GFP was also present at the ER (Figure 2C). In these cells, the Kap95-GFP fluorescence levels are 1.4 ± 0.06 fold higher at the ER compared to the cytosol ($n = 25$); a small but significant difference. As a control, we show that mCh-L-TM, a reporter that is present at the ER at approximately equal concentrations as the mCh-h2NLS-L(37)-TM reporter, but lacks the h2NLS, did not recruit Kap95-GFP at the ER in any of the analyzed cells ($n > 150$) (Figure 2D). The recruitment of Kap95 to the h2NLS-containing reporter in the ER is only seen with mCh-L(37)-TM, and not with mCh-h2NLS-L-TM (Figure 2B), because the concentration of mCh-L(37)-TM at the ER is high while that of mCh-h2NLS-L-TM is low due to efficient import. We conclude that the high-affinity NLS of the reporter proteins attract both Kap60 and Kap95 while diffusing in the ER, that is, prior to gating the NPC. The data is consistent with the strong binding of a Kap60 variant (lacking the importin-β binding domain) to h2NLS-L-GFP measured *in vitro* [K_D in the nM range; (20)] and the cellular concentrations of Kap60 and Kap95 [μmolar range; (28,29)].

Next, we measured the effect of efficient recruitment of Kap60 and Kap95 by the reporter proteins on the transport of soluble Kap60-cargo. We co-expressed the soluble cargo tcNLS-mCh, i.e. mCherry with two copies of the classical SV40 NLS (22), with GFP-h2NLS-L-TM (Figure 3A). These experiments report on the competition between soluble and membrane cargo for the pools of Kap60 and Kap95 *in vivo*. As a control, we expressed rgNLS-mCh, i.e. mCherry with the NLS of Nab2, (30,31); rgNLS-mCh makes use of Kap104 rather than Kap60 and Kap95 for nuclear import (Figure 3A). The INM accumulation of GFP-h2NLS-L-TM did not change upon co-expression with tcNLS-mCh or rgNLS-mCh (Figure 3B), but nearly all nuclear accumulation of tcNLS-mCh was lost when GFP-h2NLS-L-TM was co-expressed (Figure 3C). As anticipated nuclear accumulation of rgNLS-mCh was not affected by GFP-h2NLS-L-TM (Figure 3D). The expression level of GFP-h2NLS-L-TM (∼13 000 copies cell^{-1}) was similar to that of tcNLS-mCh (∼14 000 copies cell^{-1}) or rgNLS-mCh (∼15 000 copies cell^{-1}) (Figure S1). Thus, in the cell h2NLS-membrane cargo competes effectively with tcNLS-soluble cargo for binding to the same pool of Kap60 and Kap95.

The above data suggest that the kinetics of Kap60 and Kap95 association (and dissociation) at the ER and ONM are not likely to be rate-determining for the overall import (and efflux) of the reporter protein h2NLS-L-TM.

Lateral diffusion of membrane proteins in the ER, INM and ONM

To estimate the rate constants k_1 and k_{-1}, we analyzed the lateral mobility of the membrane reporters in the ER, the INM and the ONM, using fluorescent recovery after photobleaching (FRAP) (Figure 4A). We determined the diffusion coefficient (D) of GFP-h2NLS-GFP-L-TM,

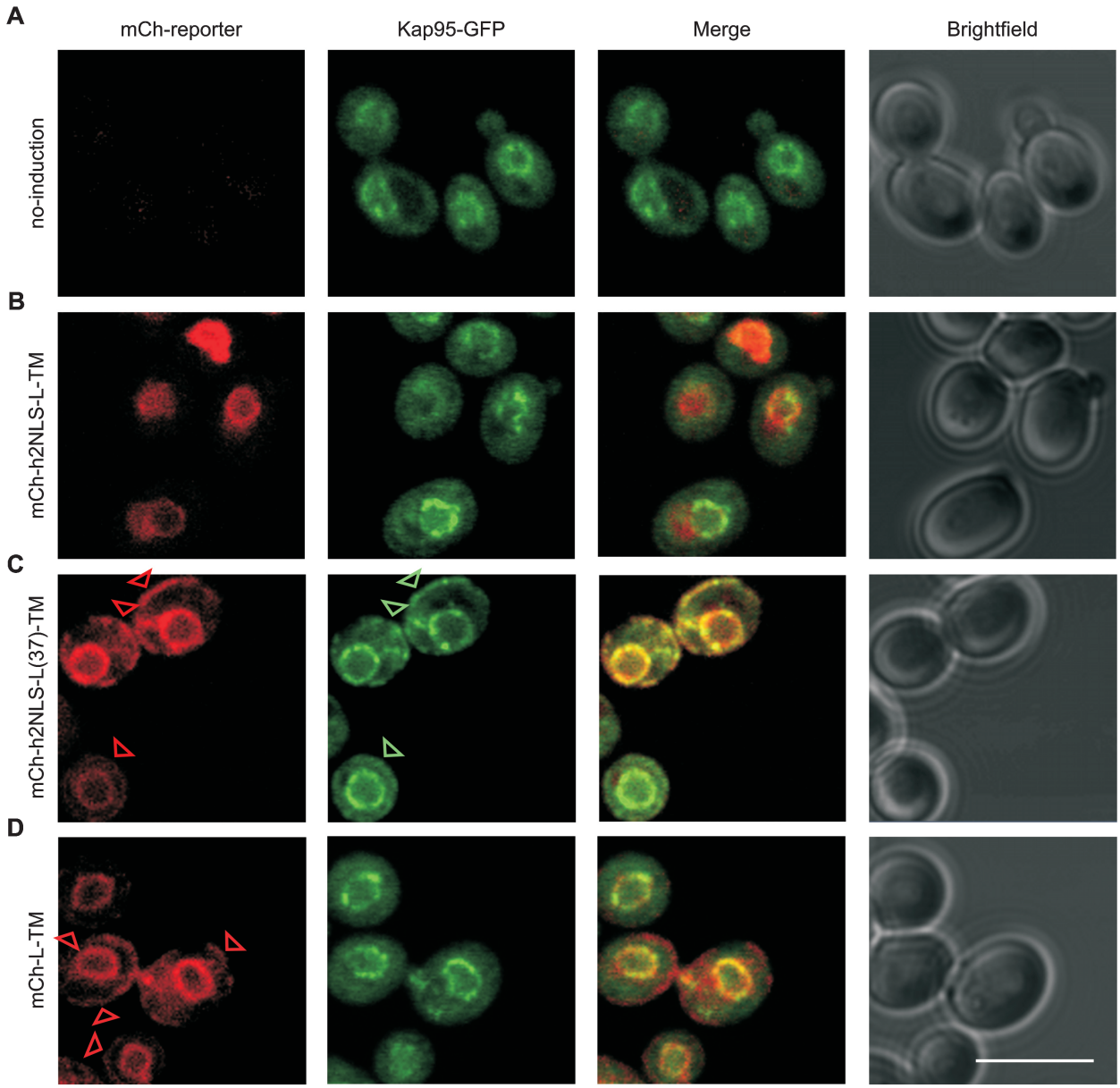

Figure 2: Kap95-GFP co-enriches with GFP-h2NLS-containing membrane reporter at the ER. Confocal images of cells expressing Kap95-GFP (A) or Kap95-GFP co-expressed with mCherry-tagged reporter proteins mCh-h2NLS-L-TM (B), mCh-h2NLS-L(37)-TM (C), or mCh-L-TM (D). In (A) the expression of mCh-h2NLS-L-TM was not induced. The red arrows indicate the location of mCh-h2NLS-L(37)-TM (C) or mCh-L-TM (D) at the ER, the green arrows indicate where Kap95-GFP co-enriches at the ER (C). Scale bar is 5 μm.

GFP-L-TM and MBP-GFP-h2NLS-L-TM. We compared the mobility of these reporters with that of ER-resident Sec translocon protein Sec61 and the full length INM-resident Heh2, both tagged with GFP. The reporter GFP-MBP-h2NLS-L-TM has an N-terminal maltose-binding protein (MBP) to increase the mass of the extralumenal domain of the membrane reporter by 40 kDa. With the additional MBP the size of the reporter is similar to that of Heh2. In order to measure the mobility at the ER, we needed a sufficiently high concentration of reporter protein at the ER, and therefore we made use of the KAP95-AA strain (32). In this strain and in the presence of rapamycin (RAP), an FRB-tagged version of Kap95 is tethered to the plasma membrane by high affinity binding to Pma1-FKBP. Addition of rapamycin thus rapidly depletes the cells of functional Kap95-FRB, and, as a consequence, the reporter proteins equilibrate over the INM, ONM and ER (20). FRAP experiments were performed at the NE or the ER and the recovery traces were fitted to an empirical equation describing the lateral diffusion of membrane proteins in one dimension through membranes (10) (Figure 4B).

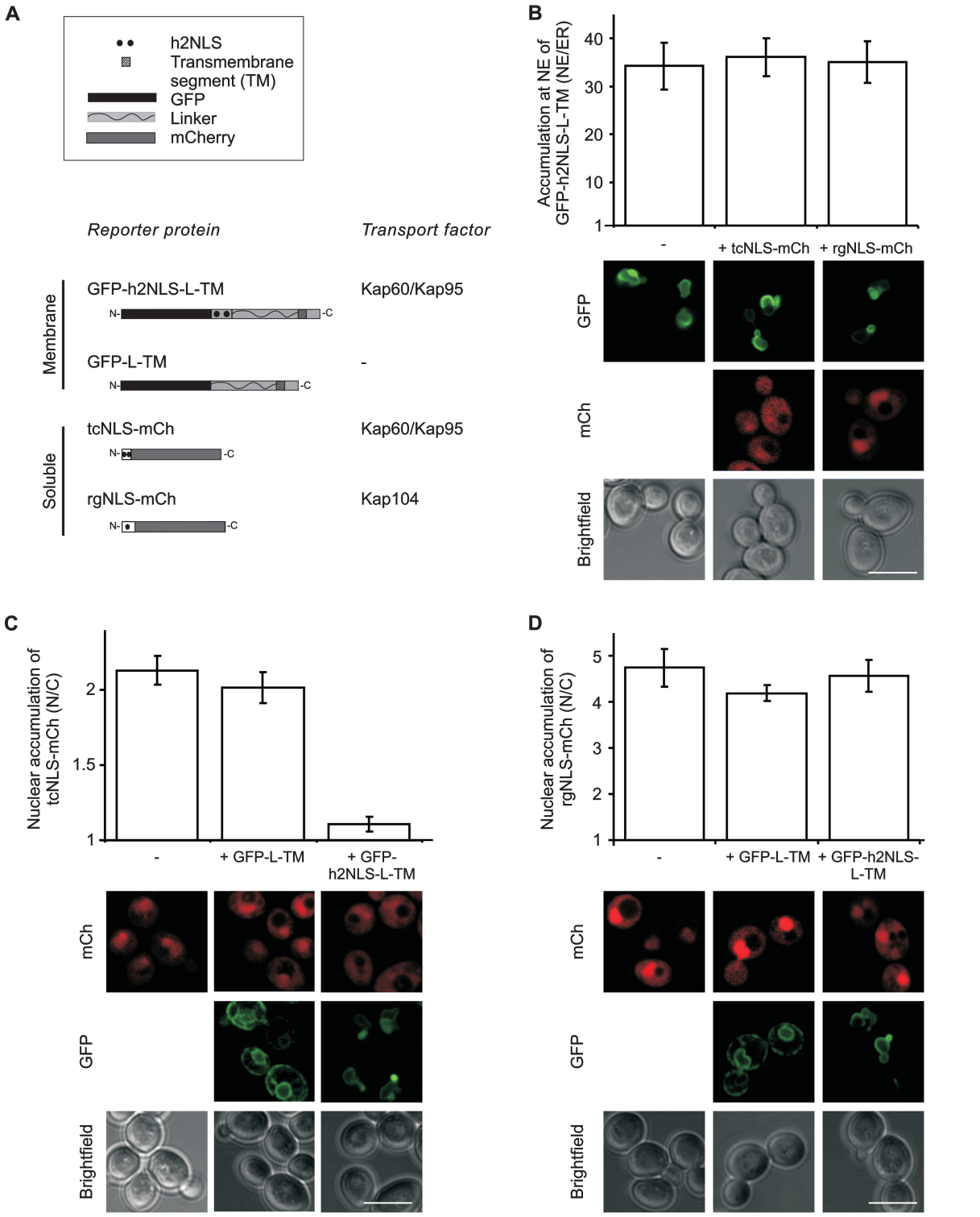

Figure 3: Nuclear transport of GFP-h2NLS-L-TM is not reduced upon co-expression of competitive cargo, tcNLS-mCherry. A) Cartoons indicate domain composition of the reporter proteins. B) The level of accumulation of GFP-h2NLS-L-TM at the INM, without co-expression (–), with co-expression of tcNLS-mCherry (tcNLS-mCh), or rgNLS-mCh ($n \geq 20$). C) The level of nuclear accumulation of tcNLS-mCh without co-expression (–), with co-expression of GFP-L-TM and with co-expression of GFP-h2NLS-L-TM ($n \geq 44$). D) The level of nuclear accumulation of rgNLS-mCh without co-expression (–), with co-expression of GFP-L-TM and with co-expression of GFP-h2NLS-L-TM ($n \geq 52$). The images show the distribution of the membrane and soluble reporters, the graphs show the quantification of the nuclear accumulation of the reporters from the top row of images. SEM, and 5 μm scale bar are indicated.

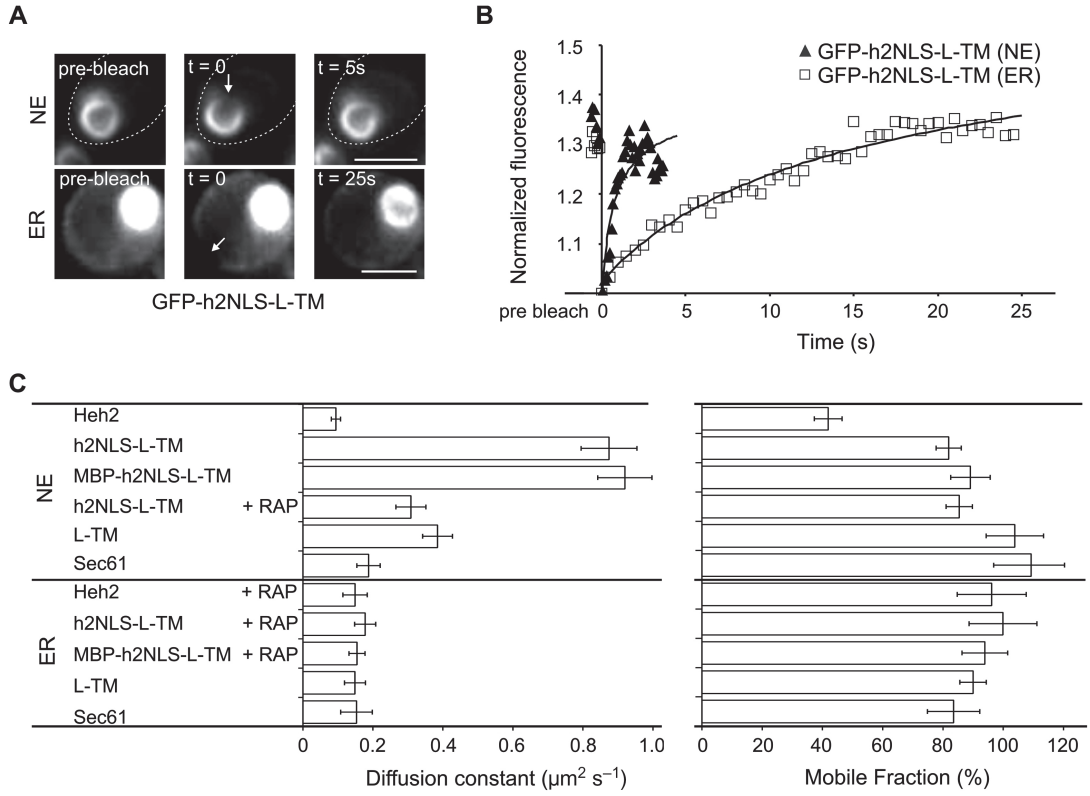

Figure 4: Mobility of reporters at the NE and ER. A) Confocal images showing fluorescence recovery after photobleaching of reporter localized at the NE (top) and at the ER (bottom). B) An example of a time-trace of fluorescence intensity in the bleached spot, for GFP-h2NLS-L-TM in the NE and ER. C) Representation of diffusion coefficients of reporters in the INM (accumulated at the NE), in the ONM (not accumulated at the NE) and in the ER (see also Table S1). All reporters are tagged with GFP. Scale bar is 2 μm, SEM is indicated.

The diffusion coefficient of all reporters and Sec61-GFP present in the ER was similar and about 0.16 $\mu m^2 s^{-1}$; the mobile fraction was in all cases >80% (Figure 4C, Table S1). The mobility of the membrane proteins was thus not sensitive to the mass of the soluble domains, which, in case of GFP-Heh2, GFP-h2NLS-L-TM and MBP-GFP-h2NLS-L-TM, also included bound-Kap60.

We measured the lateral diffusion in the INM by photobleaching the fluorescence of GFP-Heh2, GFP-h2NLS-L-TM and MBP-GFP-h2NLS-L-TM at the NE. These reporters are highly accumulated in the INM (NE/ER-ratio = 34.1 ± 4.9) and the recovery kinetics will thus be dominated by the diffusion of the INM-localized molecules. Fluorescence recovery due to transport across the NPC has little effect on the kinetics of recovery, as it is much slower. We found a fivefold higher diffusion coefficient for GFP-h2NLS-L-TM ($D = 0.87 \pm 0.08\,\mu m^2 s^{-1}$) and MBP-GFP-h2NLS-L-TM ($D = 0.92 \pm 0.08\,\mu m^2 s^{-1}$) in the INM than in the ER. In stark contrast with these high mobility values is the slow diffusion of INM resident Heh2 ($D = 0.09 \pm 0.01\,\mu m^2 s^{-1}$). The mobility of GFP-Heh2 is an order magnitude lower than that of GFP-h2NLS-L-TM and MBP-GFP-h2NLS-L-TM and the mobile fraction was ~40%, while the mobility and mobile fraction of GFP-Heh2 in the ER was similar to that of the other reporters. These findings are consistent with the observation that the majority of GFP-Heh2 is trapped at the INM (16,33), while the membrane reporters are not retained by nuclear structures (20).

We measured the lateral mobility of proteins in the ONM by photobleaching the NE in cells expressing GFP-L-TM or Sec61-GFP. These proteins are not accumulated in the INM. In addition, we used GFP-h2NLS-L-TM in the rapamycin-treated KAP95-AA strain. In the absence of functional Kap95, GFP-h2NLS-L-TM is distributed throughout the entire network of the INM, ONM and ER (20), like GFP-L-TM. We found that the diffusion coefficient of GFP-Sec61 at the ONM is similar to that of the reporters at the ER ($D = 0.19 \pm 0.03\,\mu m^2 s^{-1}$). The diffusion coefficient of GFP-L-TM ($D = 0.31 \pm 0.04\,\mu m^2 s^{-1}$) and GFP-h2NLS-L-TM (+RAP; $D = 0.38 \pm 0.04\,\mu m^2 s^{-1}$) are higher than that of Sec61 ($D = 0.19 \pm 0.03\,\mu m^2 s^{-1}$), which might relate to some contribution from the mobility of INM-localized reporters. We conclude that lateral diffusion in the ONM and ER is slower than in the INM.

In comparison, the diffusion coefficient of soluble GFP in the cytoplasm of yeast was $13.6 \pm 1.3\,\mu m^2 s^{-1}$ ($n = 20$),

which is consistent with values measured in other cell-types (34,35). Overall, we conclude that the mobility of the reporter proteins in the membranes of the ER-ONM network is almost two orders of magnitude slower than the mobility of soluble reporter proteins in the cytoplasm.

Overall efflux kinetics

To measure the kinetics of membrane protein transport we tested the three assays that have been described for measurement of transport of soluble cargo in yeast. The first is a steady state assay using selective FRAP (sFRAP). Here, one selectively photobleaches the nucleus and measures the recovery of fluorescence as a consequence of transport (import, influx and efflux) through the NPC (36,37). The second is the Kap95-depletion method. Here, the cell is depleted of functional Kap95 upon addition of rapamycin and one measures the net efflux of cargo after the import is abolished (32). The third is a metabolic poison assay were cells are treated with sodium azide plus 2-deoxyglucose to deplete the cells of metabolic energy and disrupt the RanGTP-gradient over the NPC (38,39). Immediately after poisoning net efflux can be measured and when all accumulation is lost, the metabolic poisons can be washed away, and net import can be measured. To validate the three methods, we first measured import and passive efflux of soluble GFP-tcNLS-GFP using the Kap-depletion or the metabolic poison assay methods (Figure 5A) and compared it with results from a sFRAP assay (Figure 5B) (36). Using the Kap95-depletion assay or the metabolic poison assay we directly measured the overall efflux rate constant (k_{out}) and calculated the overall import rate constant (k_{in}) from the k_{out} and the steady state accumulation of GFP-tcNLS-GFP (Figure 5A). Indeed, at steady state, the N/C ratio is equal to k_{in}/k_{out}. In the sFRAP assay, the recovery of fluorescence in the nucleus and cytosol are fitted to yield k_{in} and k_{out} (36). With all three methods, we obtained similar rate constants (k_{out} of $1.2 - 2.0 \cdot 10^{-2}$ s^{-1} and k_{in} of $0.10 - 0.16\,s^{-1}$, Figure 5C) and concluded that they are valid approaches to study NPC transport kinetics of soluble proteins. The Kap95-depletion assay offers advantages over sFRAP when nuclear accumulation is high and the pool of the cytosol-localized proteins is small which can prohibit sFRAP measurements. The Kap95-depletion method offers advantages over the metabolic poison assay as it perturbs the cell more specifically (it does not interfere with energy metabolism and ion homeostasis), but unfortunately it is not reversible.

We first aimed to measure the nuclear import of membrane proteins using sFRAP by selectively photobleaching the NE and determining the recovery of fluorescence as a quantitative measure of transport. However, due to the high accumulation of GFP-h2NLS-L-TM in the NE, a major fraction of the pool of reporter proteins was photobleached. This made the analysis very difficult. Instead, we measured the nuclear efflux rate constant of the membrane reporter GFP-h2NLS-L-TM and calculated the import rate constant, based on the efflux rate constant

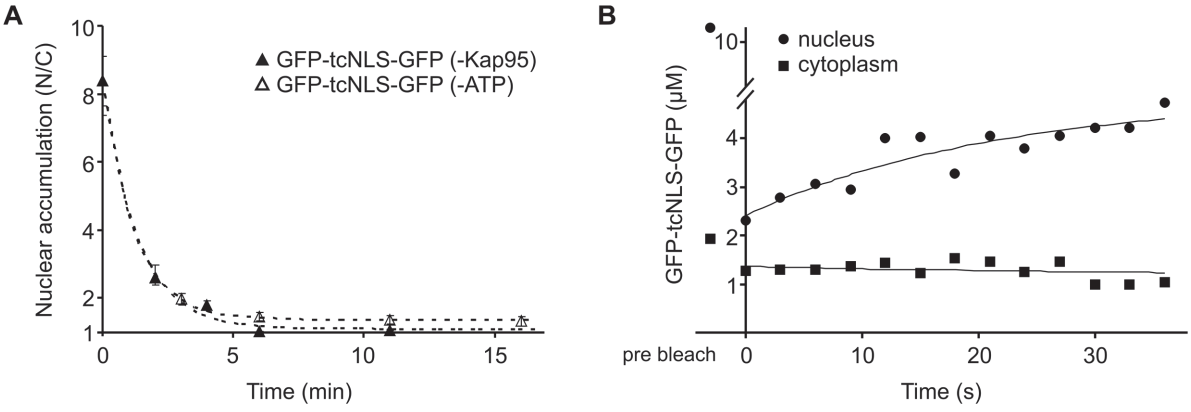

C

Nuclear transport of GFP-tcNLS-GFP

Method	k_{out} ($\times 10^{-2}$ s^{-1})	k_{in} (s^{-1})	*n*
sFRAP	2.0 ± 0.35	0.16 ± 0.029	22
Efflux (-ATP)	1.3 ± 0.15	0.11 ± 0.015	>27
Efflux (-Kap95)	1.2 ± 0.1	0.10 ± 0.011	>22

Figure 5: Comparison of Kap95-depletion and metabolic poison transport assays and selective-FRAP. A) Nuclear efflux of soluble GFP-tcNLS-GFP in the Kap95-depletion assay (▲, for each time point, $n \geq 27$) and poison assay (△, for each time point, $n \geq 22$) fitted with a single exponent (dashed line). B) Recovery traces of fluorescence from GFP-tcNLS-GFP in the nucleus (●) and cytoplasm (■) after selective photobleaching in the nucleus. Fitted as described in (36). C) Nuclear import and efflux rate constants of GFP-tcNLS-GFP, measured in different assays as indicated. *n* is the number of cells measured at each time point during nuclear efflux. In the selective-FRAP (sFRAP) assay, *n* is the number of individual selective FRAP measurements.

and the nuclear accumulation. To measure the nuclear efflux of GFP-h2NLS-L-TM in the Kap95-depletion assay, the membrane reporter was first expressed in the Kap95-AA strain and accumulated at the INM. Upon addition of rapamycin, Kap60 and Kap95-mediated nuclear import stops, resulting in a temporary net flux of GFP-h2NLS-L-TM from the INM to the ONM and ER. We plotted the NE/ER-ratio of the reporter over time and fitted the data to a single exponential. We found an overall efflux rate constant (k_{out}) of $0.83 \times 10^{-3} \pm 0.16 \times 10^{-3}$ s^{-1} (Figure 6A). Our results demonstrate that the efflux of GFP-h2NLS-L-TM is much slower in ATP-depleted cells than in Kap95-depleted cells: k_{out} of $0.15 \times 10^{-3} \pm 0.02 \times 10^{-3}$ s^{-1} (Figure 6A). The Kap95-depletion and poison assays did not show these marked differences for transport of the soluble cargo GFP-tcNLS-GFP (Figure 5A). We determined whether the ATP-dependence is specific to membrane protein efflux or may be related to just the presence of the long, unfolded linker.

We thus compared the efflux of GFP-tcNLS-GFP with a soluble reporter having the 176 amino acid-long unfolded linker of Heh2, GFP-h2NLS-L, and a reporter having a shorter linker of only 33 amino acids, GFP-h2NLS-L(33). These reporters accumulated in the nucleus more than 200-fold, due to the high affinity h2NLS [Figure 6 and (20)]. A fast and mono-exponential efflux was observed for all three reporters after the cells were depleted of Kap95 (Figure 6B,C). The efflux of the larger GFP-h2NLS-L was somewhat slower than GFP-h2NLS-L(33), as expected.

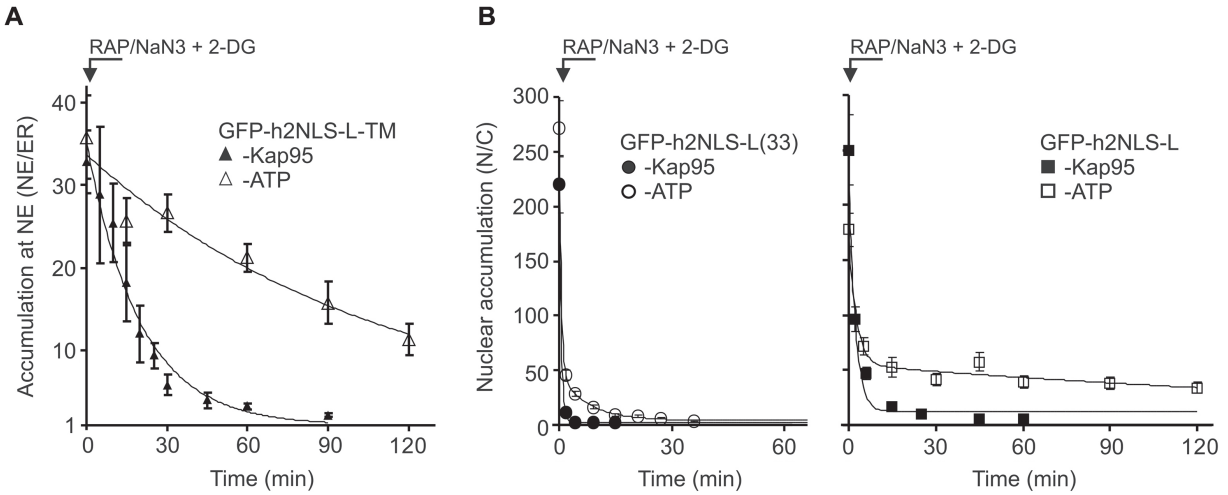

C

		-Kap95		-ATP			
	Size (kD)	k_{out} (s^{-1})	R^2	k_{out} (s^{-1})	$k_{out}1$ (s^{-1})	$k_{out}2$ (s^{-1})	R^2
GFP-h2NLS-L(33)	37	18×10^{-3}	0.999	11×10^{-3}	–	–	0.998
GFP-h2NLS-L	53	7.7×10^{-3}	0.987	–	6.5×10^{-3}	0.067×10^{-3}	0.987

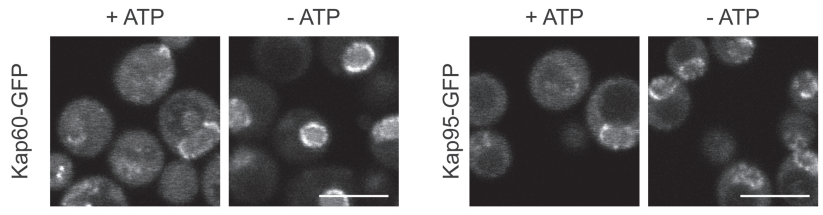

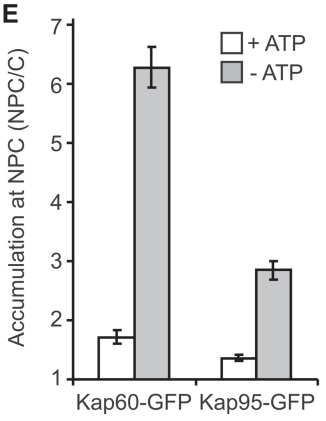

Figure 6: Measurements of nuclear efflux of membrane and soluble reporter proteins by depleting the cells of Kap95 or ATP. A) After the expression of GFP-h2NLS-L-TM, the cells were depleted of functional Kap95 [▲, data from (20)] or ATP (△) after rapamycin (RAP) or sodium azide plus 2-deoxyglucose (NaN_3 + 2-DG) was added. The nuclear accumulation (NE/ER) was plotted as a function of time and fitted to a single exponent (dashed line). ($n < 8$ for each time point). B) Similar as (A), cells were depleted of functional Kap95 [data from (20)] or depleted of ATP, after expression of GFP-h2NLS-L(33) (●/○) or GFP-h2NLS-L (■/□). The nuclear accumulation (N/C) is plotted as a function of time and fitted to a single exponent (dashed line) ($n < 14$). The nuclear efflux of GFP-h2NLS-L in the metabolic poison assay (□) was fitted with a two-term decay model. C) The nuclear efflux rate constants measured in the Kap95-depletion assay and in the poison assay and the R^2 for each fit. D) Confocal images of Kap60-GFP and Kap95-GFP, under normal conditions (+ATP) and depletion of ATP (−ATP). E) The accumulation at the NPC of Kap60-GFP and Kap95-GFP under normal conditions (open bars) and in cells depleted of ATP (gray bars). Scale bar is 5 μm, SEM is indicated.

However, a marked difference was observed when the cells were depleted of ATP. Initially, the efflux of GFP-h2NLS-L was fast but it levelled off after a few minutes (Figure 6B). The data could not be fitted with a mono-exponential decay fit ($R^2 < 0.6$) but was fitted by a two-term exponential decay model, which yielded two first-order rate constants for efflux. The efflux of GFP-h2NLS-L(33) in ATP-depleted cells could be fitted by a mono-exponential decay. The efflux rate constant of the initial fast phase for GFP-h2NLS-L did not differ significantly from the value in the Kap95-depletion assay (Figure 6C). We conclude that the linkers do not affect the nuclear efflux of soluble reporters when the cells contain normal ATP levels, but do so under energy-depleted conditions.

What could be the molecular basis for these observations? Upon ATP depletion, the Kap-cargo complexes do not dissociate from the nuclear face of the NPC in the absence of a RanGTP-gradient (40,41). Kap-cargo stuck in the NPC would obstruct further nuclear efflux (42). Indeed, when we image the localization of Kap60-GFP and Kap95-GFP, we see that they concentrate at the NPCs upon addition of sodium-azide plus 2-deoxygluces. In wild-type cells, Kap60-GFP and Kap95-GFP show the punctuate fluorescence stain, typical for NPC-localized proteins (Figure 6D). After ATP depletion, the ratio of fluorescence at the NPC over the intensity in the cytoplasm (NPC/C) increased seven- and fivefold for Kap60 and Kap95, respectively (Figure 6E). We thus confirm previous data (41) and show that the Kap-cargo complexes accumulate at the NPC in ATP-depleted cells. The NPC-accumulated Kap-cargo might particularly hinder the nuclear efflux of molecules with large Stokes radii, such as the linker-containing reporters. The high-affinity h2NLS on the soluble reporters may be bound by NPC-resident Kaps, which provides an extra means of retention in the NPC during nuclear efflux. In conclusion, as we see similar effects of ATP depletion for the efflux of soluble and transmembrane reporters, it is most likely that the slow efflux of GFP-h2NLS-L-TM in the absence of ATP is simply due to the presence of the h2NLS-L domain with large Stokes radius and not specific for membrane transport. The ATP-depletion assay is thus not suitable to determine efflux rate constants of h2NLS-L-TM.

Efflux of reporters with large extralumenal domains

Where does the NLS-terminal region of membrane reporters pass through the NPC during efflux? To address this question we increased the number of soluble domains at the N-terminus and thus the mass and Stokes radius of the proteins. If the extralumenal domains of the reporters travel through the narrow lateral channel facing the POM, one would expect a slowing of the efflux with increasing mass. In fact, the upper size limit for transit through the lateral channel in yeast or vertebrate NPCs is thought to be ~60 kDa (8,13,43). We observed that reporters with extralumenal domains of 174 kDa are capable to travel from the INM to ONM/ER (Figure 7A). The rate constants for efflux were constant (k_{out} ~0.9×10^{-3} s^{-1}) up to an extralumenal domain mass of 92 kDa and decreased to 0.15×10^{-3} s^{-1} at 174 kDa (i.e. three additional MBP-domains). The expression of the reporters MBP-GFP-MBP-h2NLS-L-TM and MBP-GFP-2×MBP-h2NLS-L-TM showed spots with high fluorescence intensity at the NE in a fraction (<20%) of the cells, which did not disappear upon addition of rapamycin. These sites may correspond to reporter aggregation at the INM and/or ONM, and as a result, the efflux rate constant will be underestimated. In parallel with a fivefold reduced exit rate, the nuclear accumulation (NE/ER ratio) decreased with increasing number of soluble domains (Figure 7B). This implies that the overall import was affected more than the efflux (Figure 7B,C). Altogether, the efflux kinetics of the reporter with multiple extralumenal domains is not compatible with passage through 10 nm wide lateral channels (14) and argue for a spacious exit route, alike that is used during import.

Discussion

The yeast membrane protein Src1/Heh1 and Heh2 pass the NPC via an import mechanism that depends on the interactions between Kap95 and FG-Nups to cross the central channel of the NPC (16,20). A long intrinsically disordered linker spacing the h2NLS and the transmembrane domain facilitates the interactions between NLS-associated Kaps and FG-Nups. We now present a quantitative analysis of Kap60 and Kap95-mediated import and efflux of membrane cargos, including data on the mobility of the reporter proteins in the different membrane compartments.

Lateral diffusion in the INM, ONM and ER

Our estimates of lateral diffusion of membrane proteins in the ER of yeast, full length as well as the reporter proteins (Figure 4) are a little lower than those in the mammalian ER, where values ranging from 0.3 to 0.5 $\mu m^2 s^{-1}$ were measured (10,12,44) and similar to the half-times of recovery measured for full length proteins in the ER of HeLa cells (45) (corrections for different sized areas of the bleaching spots were taken into account).

The low diffusion coefficient of GFP-Heh2 at the INM is comparable with earlier findings of other full length membrane proteins trapped at the INM (10,12) and concur with those of proteins tested in HeLa cells (45). The diffusion of INM proteins is much slower than that of our reporter proteins in the INM. These differences are likely caused by (transient) interactions of the full-length proteins with other nuclear structures, while our reporters in yeast were designed to assure free diffusion.

The diffusion of the free moving membrane reporters in the ER and ONM were observed to be five to six times slower than in the INM (Figure 4). Overall, the diffusion in

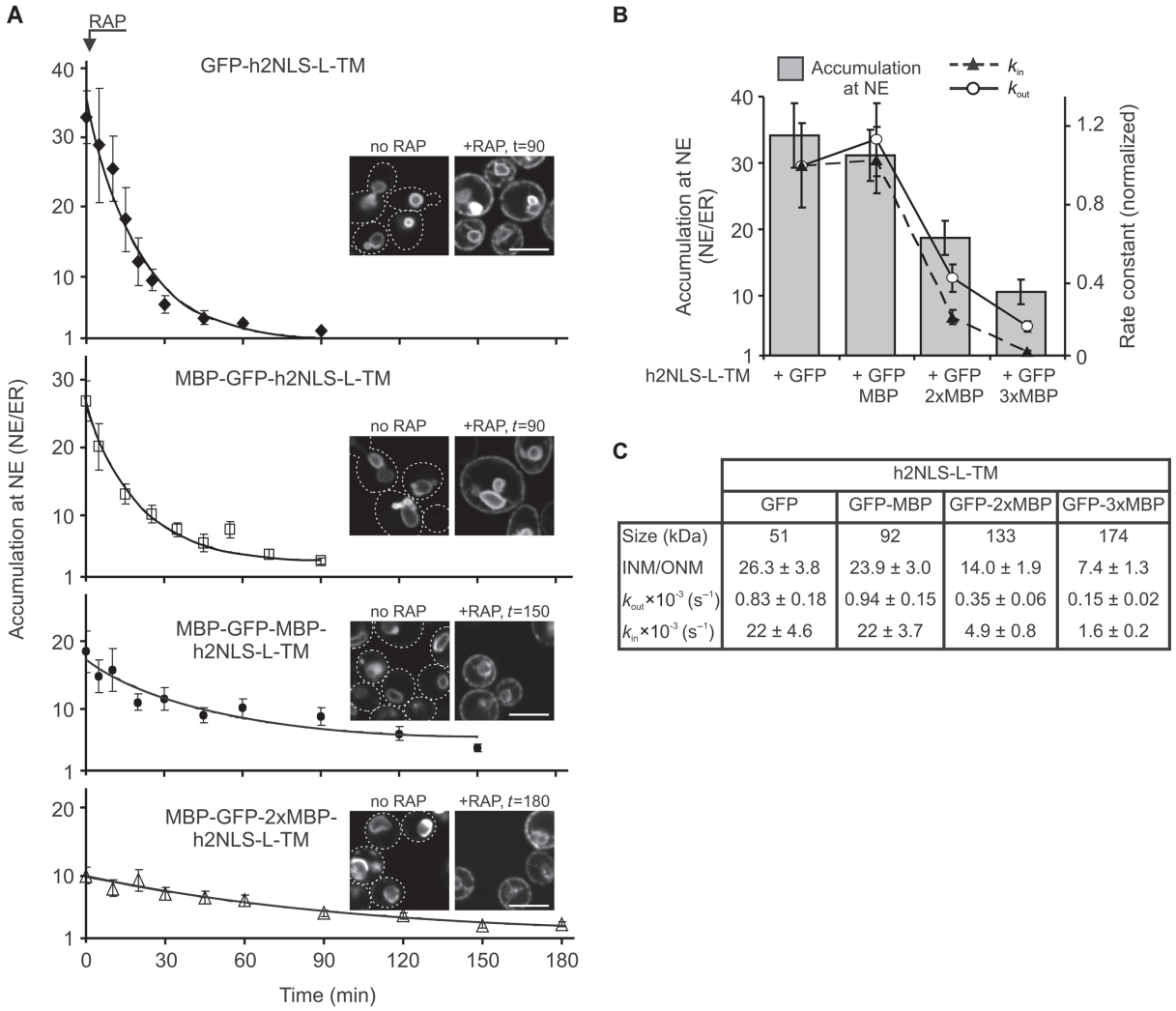

C

	h2NLS-L-TM			
	GFP	GFP-MBP	GFP-2xMBP	GFP-3xMBP
Size (kDa)	51	92	133	174
INM/ONM	26.3 ± 3.8	23.9 ± 3.0	14.0 ± 1.9	7.4 ± 1.3
$k_{out}\times10^{-3}$ (s^{-1})	0.83 ± 0.18	0.94 ± 0.15	0.35 ± 0.06	0.15 ± 0.02
$k_{in}\times10^{-3}$ (s^{-1})	22 ± 4.6	22 ± 3.7	4.9 ± 0.8	1.6 ± 0.2

Figure 7: Large extralumenal domains can transit via the central channels of the NPC. A) The nuclear accumulation (NE/ER) of GFP-h2NLS-L-TM [◆, data from (20)] and of reporters with one (□), two (●) or three (△) additional extralumenal MBPs is plotted as a function of time upon addition of rapamycin and fitted with a single exponent. Confocal images of the cells at indicated time points are shown. B) The nuclear accumulation (NE/ER) at steady state of GFP-h2NLS-L-TM and the derived variants with one, two or three additional extralumenal MBPs [bars, data from (20)]; the overall efflux rate constants (k_{out}, ○, solid line) and overall import rate constants (k_{in}, ▲, dashed line) derived from (A) are also plotted. C) The overall efflux rate constants (k_{out}) and the calculated overall import rate constants (k_{in}). SEM, and 5 μm scale bar are indicated.

the ONM and ER of the yeast cell was thus lower than in the INM, possibly reflecting a higher macromolecular crowding in the ONM and ER and/or a different viscosity of the membrane (e.g. lipid composition). We note that overexpression of INM (reporter) proteins can trigger membrane proliferation (16,20), and this may also cause the differences in diffusion constants measured in the INM and ONM.

Quantitative analysis of active and passive transport of membrane cargo

The diffusion of membrane proteins in the ER was almost two orders of magnitude slower than the diffusion in the cytosol of yeast. For the lateral diffusion of GFP-h2NLS-L-TM through the membranes of the ER, a diffusion coefficient of $D = 0.16\,\mu m^2\,s^{-1}$ was measured. The diffusion through the membranes (k_1 and k_{-1}) may thus have a significant influence on the overall import. If we estimate that the reporter diffuses on average 3.5 μm from a position in the ER to an NPC (see *Materials and Methods* for this estimation), it would take ∼20 s based on a 2D random walk. This number is indeed in the same range as the half time for import (∼31 s) that can be calculated on the basis of the $k_{in} = 2.2 \times 10^{-2}\ s^{-1}$ (see below).

For estimates of the ratio between the concentrations of the reporters at the INM and the ONM, we considered a simplified view of what we know of the structure of

the ER at the periphery of a yeast cell (46) and assume it consists on average of cisternae of two closely positioned bilayers enclosing the lumenal space, alike the NE. Furthermore, we assume that 40% of the periphery is covered with ER [between 20–40% (46,61)]. Lastly, we assume that the concentrations of the reporter in the two membranes of the ER and in the ONM are identical. With these assumptions we can convert our measured NE/ER ratio of 2.3 of GFP-L-TM (20) into an INM/ONM-ratio of 0.8. GFP-h2NLS-L-TM with a measured NE/ER ratio of 34 converts to an INM/ONM ratio of 26. If efflux is limited by passage over the NPC, then $k_{out} = k_{-2}$, and we can calculate an import rate constant k_3 for GFP-h2NLS-L-TM of $\sim 2.2 \times 10^{-2}$ s^{-1} from the measured efflux rate constant of 0.83×10^{-3} s^{-1} and the INM/ONM ratio of 26.

In conclusion, with the assumptions made, our measured efflux rate constants and rates of lateral diffusion point towards efflux over the NPC being at least an order of magnitude slower than Kap-mediated import. Also, for Kap-mediated import, the actual transport through the NPC is likely not rate-limiting as diffusion through the ER-ONM is slow.

Comparing transport of soluble and membrane cargo through the NPC

From Western blot analysis (Figure S1A,B), we estimated that about 13×10^3 membrane reporter molecules are present per cell. Taking into account the accumulation ratios and estimates of the surface area of the INM, ONM and ER membranes (see *Materials and Methods* for details), we find $\sim 0.4 \times 10^2$ molecules μm^{-2} in the ONM and ER and $\sim 8.8 \times 10^2$ molecules μm^{-2} in the INM. With these estimates 80% of the molecules would be at the INM. Assuming a density of 12 NPCs per μm^2 (31,47), the flux of GFP-h2NLS-L-TM over the NPC is ~ 0.06 molecules/NPC $\times$ s.

How do these fluxes compare to those of soluble nuclear transport? For the soluble reporter GFP-tcNLS-GFP, we found an import rate constant of 0.16 ± 0.03 s^{-1} (Figure 5). We estimated $\sim 1.5 \times 10^5$ copies of soluble GFP-tcNLS-GFP in the cytoplasm, yielding a flux of soluble reporters over the NPC of 13 ± 2.2 molecules/NPC $\times$ s, which is in good agreement with earlier studies in yeast (31). If the GFP-tcNLS-GFP reporter would be present at an equal number of copies per cell as GFP-h2NLS-L-TM, the flux would have been 1.5 molecules/NPC $\times$ s. This is more than an order of magnitude faster than the flux of ~ 0.06 molecules/NPC $\times$ s for GFP-h2NLS-L-TM.

In conclusion: by comparing the transport kinetics of Kap60 and Kap95-facilitated import of the integral membrane reporter GFP-h2NLS-L-TM and soluble GFP-tcNLS-GFP, we note the following: (i) the affinity of Kap60 for the h2NLS of the membrane reporters is high and as a consequence there is little competition with 'low-affinity' soluble cargos; (ii) the lateral diffusion in the ER is slow, and the path long, and this may significantly affect the overall nuclear import kinetics; (iii) the tcNLS and other NLS's have a lower affinity for Kap60 than h2NLS, and finding a Kap may have major impact on the overall import rate of soluble cargos (31); and (iv) the diffusion of soluble cargo in the cytoplasm is relatively fast and not rate-limiting for the nuclear import (31,48). The relatively slow but robust accumulation of membrane cargo is compatible with reported roles of actively imported INM proteins, such as NPC-assembly and maintenance of nuclear organization and structures (17–19,33,49–53).

Lastly, we observed a decreased efflux through the NPC upon ATP depletion for both soluble and transmembrane reporters that have the linker domains with large stokes radii and the h2NLS (Figure 6). ATP depletion increases the residence of Kap60 and Kap95 at the NPC [Figure 6E and (41)] increasing crowding in the NPC. The inhibition of efflux was more pronounced with the membrane reporter protein than with the soluble reporter proteins, so crowding in the NPC may affect the membrane reporters more. Alternatively or additionally, the linker adopts different conformations, more compact in the soluble GFP-h2NLS-L than in the membrane reporter protein GFP-h2NLS-L-TM due to the extended linker while in transit.

Mechanism of transport across the NPC of membrane cargo

On the basis of the here presented and our published work (20), we discuss a possible mechanism and path for transport of membrane proteins through the NPC. Our previous data support the view that the extralumenal domains of the investigated INM-destined membrane proteins are transported through the central channel of the NPC (20). Most conclusive is that we show that the N-terminal moiety of the linker can be trapped at the Nsp1-anchor site. Our present data suggests that the extralumenal domains terminal to the linker can travel back to the ONM through the same channel. Namely, we found that membrane reporters could leak back from the nucleus to the ER, while having extralumenal domains with overall masses far above the reported upper size limit for proteins diffusing through the lateral channel facing the POM (Figure 7A). Vice versa, we expect that the reporter with large extralumenal domains terminal to the linker can also reach the INM by influx, with similar slow kinetics.

We had proposed that the NPCs have a central channel that is continuous with narrow conduits through the scaffold, lateral gates. These gates enable the linker to slice through the scaffold of the NPC. Since these lateral gates have not been detected in electron microscopy studies (14,54–57), they may be narrow, likely dynamic and possibly existing after restructuring of the NPC (58), but wide enough for a linker to slice through. One possibility is that such gates are formed in-between the eightfold rotational symmetry units, the spokes, of the NPC (14,57).

During nuclear import of membrane proteins, the karyopherin-bound NLS interacts with FG-repeat binding sites in the NPC, which may favour a stretched or extended conformation of the flexible linker. We infer that it would not cost much energy to promote this extended conformation, as intrinsically disordered domains can already adopt a wide range of conformations (59) and are typically less stiff than folded domains (60). With both ends of the molecule 'bound', the TM domain embedded in the membrane and the NLS bound to the FG-repeats via Kap60 and Kap95, the linker can dodge into the lateral gates. The length of the linker may give the karyopherin enough freedom to scavenge the entire width of the central channel and interact with the numerous FG-repeats. The RanGTP-gradient gives direction to the flux of Kap-cargo to the nuclear site of the NPC. Without karyopherins attached to the NLS, entry into the NPC, and residence of the extralumenal domain in the central channel, will be much less likely to occur. Due to the intrinsic dynamics of the linker, it will still occasionally adopt an extended conformation, and the soluble domains terminal of the linker can enter the NPC central channel and allow efflux of the reporter. Future studies will have to show if the interpretation of our data is correct. Key will be to show the existence of the lateral gates connecting the space immediately adjacent to the nuclear envelope and the central channel with more direct methods.

Materials and Methods

Strains and plasmids. All experiments were performed in the *S. cerevisiae* KAP95-AA strain derived from W303 (20,32), except for the selective-FRAP measurements (Figure 5), and the localization experiments (Figure 2), which were performed in a BY4742 background [(61), Invitrogen]. The correct integration of GFP in the strains Sec61-GFP, Kap60-GFP and Kap95-GFP [(62), Invitrogen] was confirmed by PCR. The plasmids were obtained according to standard cloning techniques, see supplementary material for details. The strains and plasmids are listed in Table S1 and S2.

Growth conditions. Yeast strains were grown at 30°C in synthetic dropout medium without histidine, leucine and/or uracil, supplemented with 2% (w/v) filter-sterilized D-raffinose or D-glucose plus 0.01% (w/v) adenine. The genes encoding membrane reporter proteins were expressed from low-copy plasmids, based on pUG34 and pUG35 (63), under the control of the *GAL1* promoter, in cells cultured in medium supplemented with D-raffinose. The membrane reporter genes were induced with 0.1% (w/v) D-galactose in 2 h, the mCh-reporters and MBP-GFP-MBP-h2NLS-L-TM were induced in 3 h and MBP-GFP-2×MBP-h2NLS-L-TM in 4 h. The soluble protein GFP-tcNLS-GFP was expressed under control of a constitutive *MET25* promoter from a pUG34 plasmid and the soluble proteins rgNLS-mCh and tcNLS-mCh were expressed from a 2μ-plasmid under the control of the *TPI1*-promoter, based on pBT016-Nab2NLS-GFP-PrA (31). The cells expressing the soluble reporters were grown in medium supplemented with 2% (w/v) D-glucose.

Fluorescence microscopy

Image acquisition: All imaging and selective-FRAP experiment were performed on a home-build laser-scanning confocal microscope or a commercial LSM 710 confocal microscope as described previously (20). Data was analyzed with home-made software and the ZEN2010B package (Carl Zeiss). To quantify the protein mobility in the membranes, an epi-fluorescence microscope was used, which is based on an inverted microscope Observer D1 (Carl Zeiss). The laser beam (488 nm, argon ion laser, Melles Griot) was focused by a Zeiss C-Apochromat infinity-corrected 1.2 NA 63× water immersion objective and directed to the sample. The fluorescence emission was detected by a Cool-Snap HQ2 CCD camera (Photometrics) and recorded in MetaMorph (Molecular Devices).

Data analysis and NE/ER-ratios. Since the resolution of optical microscopy does not discriminate the INM from ONM, we used the NE/ER ratio as a measure for accumulation at the INM. The NE/ER ratio is an experimental value that allows direct comparison of import efficiencies. The NE/ER ratio was calculated as the average pixel intensity at the nuclear envelope (NE) divided by the average pixel intensity at the peripheral or plasma membrane associated endoplasmic reticulum as described before [(20), and in supplementary material]. We previously showed that the NE/ER-ratios are stable over hours after induction of expression and confirmed that the ratios are determined reproducibly despite manual selection of regions of interest and thresh holding.

The nuclear transport of membrane proteins across the NPC is between the ER-ONM network and the INM. We assume that the concentrations at the ER and ONM are the same. The changes in membrane protein density at the INM ($[A]_{INM}$) and ER-ONM ($[A]_{ER/ONM}$) can be written as:

$$\frac{d[A]_{INM}(t)}{dt} = k_{in}[A]_{ER/ONM} - k_{out}[A]_{INM} \quad (1)$$

$$\frac{d[A]_{ER/ONM}(t)}{dt} = -k_{in}[A]_{ER/ONM} + k_{out}[A]_{INM} \quad (2)$$

where k_{in} and k_{out} are the import and the efflux rate constants, respectively, and t is the time. At steady state is the reporter concentrations at the INM ($[A]_{INM}$) and the ONM ($[A]_{ONM}$) determined by the ratio of k_{in}/k_{out} (eqn 3)

$$\frac{[A]_{INM}}{[A]_{ER/ONM}} = \frac{k_{in}}{k_{out}} \quad (3)$$

The INM/ONM ratio, the ratio of the reporter concentrations at the INM and the ONM, is calculated from the experimental NE/ER ratios, the measured ratio of fluorescence levels at the NE and the ER. First, for the purpose of our calculations we consider that the ER consists on average of two closely positioned bilayers forming cisternea (flattened membrane disks) enclosing a lumen that is continuous with the NE lumen. This is obviously a simplification as the structure of the ER is more complex, consisting of cisternae (flattened membrane disks) and tubules (tube structures) (46). Second, proteins can diffuse throughout the entire network, and we assume that the concentration of membrane reporters in ONM and ER are equal. Third, to estimate the concentrations of the reporters and the surface area of the ER membranes, we take into account that 40% of the plasma membrane is covered with peripheral ER at the contour of a yeast cell [20–40% in (46,64)]. At our resolution, we see the ER as a continuous membrane system, so when assuming the ER covers 40% of the contours of the cell, the actual concentration of fluorescent reporters at the ER is underestimated by a factor of 2.5 times when simply measuring the average fluorescence intensity. To correct for this, we calculate as follows: We measured for GFP-h2NLS-L-TM an NE/ER-ratio of 34, thus for the fluorescence *intensities* (i) in the membranes we can write: $i(NE):i(ER) = 34:1$. Not taking into account the 2.5 times underestimation of the concentration at the ER and ONM we would write $i(INM):i(ONM):i(ER) = 33.5:0.5:1$. But correcting for this underestimation of the concentration of reporters at the ER and ONM, we can write for the ratio of *concentrations* of reporters in the INM and ONM: $INM/ONM\ ratio = (i(NE):i(ER) - (0.5 \times 2.5))/(0.5 \times 2.5) = 26$. For GFP-L-TM, with a measured NE/ER-ratio of 2.3, we arrive at an INM/ONM-ratio of 0.84.

Diffusion of soluble protein. We used a LSM710 confocal microscope to measure the diffusion coefficient of GFP in the cytoplasm. We positioned

the focused laser beam (wavelength: 488 nm) in the cytoplasm of a yeast cell and photobleached a small spot for 3.31 ms with 100% of the output power of a 15 mW solid state laser to obtain 40–50% of the initial intensity. The recovery was measured by taking images of $0.5 \times 0.5\,\mu m$ in the bleached spot every 3.78 ms for a period of 200 ms using 0.4% of the output power of the laser. The recovery trace was fitted to a single exponent to find the half-time of recovery. The diffusion coefficient was obtained according to eqn 4, derived from (65):

$$D = \frac{w^2}{4t_{0.5}} \tag{4}$$

where D is the diffusion coefficient, w the radius of the beam and $t_{0.5}$ the half-time of recovery. To determine the diameter of the beam, we bleached a similar spot in poly(methyl methacrylate) (PMMA) doped with Rhodamine B, imaged a frame of $5 \times 5\,\mu m$ and measured the diameter (d) of the beam as the full width at half minimum (FWHM) of the spot, yielding $d = 2.0 \pm 0.2\,\mu m$ ($n = 16$).

Lateral diffusion of membrane proteins. For quantitative estimates of protein mobility in the membrane, FRAP-measurements were performed. The laser was focused for 30–50 ms to photobleach the fluorescent signal at the membrane to 40–50% of the initial intensity, using ~10% of the output power of a 10 mW argon ion laser. Immediately after the photobleaching, a time series of 50 images was recorded every 100 ms during 3.7 min for fast diffusing reporters at the INM or 500 ms during 25 min for the more slow lateral diffusion in the ONM and ER. The diameter (d) of the photobleached spot was defined as the full width of half minimum (FWHM) of the intensity level immediately after photobleaching and determined as $d = 1.8 \pm 0.1\,\mu m$ ($n = 38$).

The fluorescence intensity was determined by pixel analysis in the centre of the photobleached spot ($d = 0.7\,\mu m$), using MetaMorph (Molecular Devices). A significant fraction of total fluorescence at the NE was photobleached, since we photobleached a spot corresponding to 20–40% of the size of NE. To find the mobile fraction, we corrected for this reduction of the total fluorescence by plotting the ratio of the intensity in the bleached spot over the intensity in a reference spot with the same size at the same membrane compartment. The photobleaching as a result of imaging during the recovery was negligible (~4%). Therefore, uncorrected data could be fitted according to earlier publications (10) to obtain a measure for the lateral diffusion coefficient D (expressed in $\mu m^2\,s^{-1}$).

We estimated how much time a membrane protein would need on average to diffuse from the ER to the nucleus. We used eqn 5 for the mean squared displacement, describing the average distance (r) a particle travels in time (t) based on Brownian motion of a random walk in a two dimensional system of the plane of a membrane.

$$\left\langle r^2(t) \right\rangle = 4Dt \tag{5}$$

D is the coefficient for lateral diffusion and t is the time interval. We measured the volume of a yeast cell as $49 \pm 2\,\mu m^3$ ($n = 381$) (36), consistent with (66). We calculated a circumference of a yeast cell of ~14.3 μm, and we estimated the average travel distance (r) through the peripheral ER aligning the plasma membrane to be approximately a quarter of the cell's circumference, being ~3.5 μm.

Selective-FRAP. Selective-FRAP was used to quantify the nuclear transport of soluble proteins [as reviewed in (37)]. The import and efflux rate constants of soluble proteins were calculated as described before (36).

Reporter efflux assays. (i) The Kap95-depletion assay: After 2 h of reporter protein expression in exponentially growing KAP95-AA cells, $2\,\mu g\,mL^{-1}$ of rapamycin was added to trigger Kap95-FRB interaction with Pma1-FKBP. Kap95 depletion disables further Kap95-mediated nuclear import, resulting in a net efflux of INM-accumulated reporter (20,32). (ii) The poison assay: The cells were harvested and resuspended in glucose-free medium supplemented with 10 mM sodium azide plus 10 mM 2-deoxy-D-glucose. This treatment dissipates the ATP pool and thereby the Ran-GTP gradient across the nuclear envelope. For both assays, images at $t = 0$ were recorded, i.e. before adding rapamycin or sodium azide/2-deoxy-D-glucose, and time series were recorded for a period of 90–180 min. The cells were kept at 30°C during the course of the experiment. For every time point new microscopy slides were prepared from one culture, the data thus represents averages of multiple cells.

We plotted the nuclear accumulation as the NE/ER ratio and fitted the data with a single exponential decay function. We simplified eqn 1 to obtain eqn 6 as the passive inward flux is negligible during the efflux experiment.

$$d\frac{[A]_{INM}}{[A]_{ONM/ER}} = -k_{out}\frac{[A]_{INM}}{[A]_{ONM/ER}}dt \tag{6}$$

or a two-term exponential decay function:

$$d\frac{[A]_{INM}}{[A]_{ONM/ER}} = \left(-k_{out\,1}\frac{[A]_{INM}}{[A]_{ONM/ER}} - k_{out\,2}\frac{[A]_{INM}}{[A]_{ONM/ER}}\right)dt \tag{7}$$

Calculation of import rate constants and membrane protein fluxes through the NPC. The import rate constant was calculated from the steady state accumulation of the membrane reporter and the efflux rate constant as estimated in the Kap95-depletion, using eqn 4. The import rate constant was used to calculate the flux of reporter through the NPC (in units of molecules/NPC × s), which requires an estimate of the number of reporters per cell, the total surface area of the ER-ONM and the INM, and the number of NPCs per nucleus. Quantitative Western blotting yielded a copy number of GFP-h2NLS-L-TM in the Kap95-AA strain of ~13 000 per cell (Figure S1A,B). On the basis of the geometry of the cell, we estimated the average radius of the cell and nucleus as $r = 2.3 \pm 0.1\,\mu m$ and $r = 1.00 \pm 0.05$ ($n = 381$), respectively, as described in (36). Assuming the ER as a double membrane and aligned with the outline of the cell and covering ~40% of the plasma membrane (46,64), we estimated the surface area of the ER-ONM to be $\sim 64\,\mu m^2$ and that of the INM $\sim 12\,\mu m^2$, which is consistent with earlier data (67,68). The density of NPCs in the NE of yeast is on average 12 NPCs/μm^2 (31,47). Given the accumulation of GFP-h2NLS-L-TM at the INM, and assuming equal concentrations of reporter in ONM and ER, we calculated a membrane protein density for GFP-h2NLS-L-TM of 879 NPCs/μm^2 at the INM and 39 NPCs/μm^2 at the ER-ONM in the Kap95-AA strain.

Acknowledgments

We thank V. Krasnikov for help with microscopy, G. van den Bogaart, P. Popken and A. Kralt for help with data analysis. This work was supported by funding from the Netherlands Organization for Scientific Research NWO (VIDI fellowship to L. M. V. and top-subsidy grant 700.56.302 to B. P.). L. M. V. and A. C. M. designed the experiments. A. C. M. performed the experiments. A. C. M., B. P. and L. V. wrote the paper.

Supporting Information

Additional Supporting Information may be found in the online version of this article:

Appendix S1: Plasmid construction.

Figure S1: The expression levels of the reporter protein GFP-h2NLS-L-TM. A) The copy number of GFP-h2NLS-L-TM was obtained from quantitative Western blots using an antibody against GFP or mCherry. The culture was grown to a density of 1.7×10^7 cells mL^{-1} and the expression of GFP-h2NLS-L-TM was induced for 2 h with 0.1% (w/v) D-galactose. An equivalent of 8.3×10^6 cells was loaded on a SDS-PAA gel together with a dilution series from 25 to 800 fmol of purified GFP and the proteins. B) We used chemiluminescence to detect the proteins

and densitometry to quantify the protein levels. We found 180 fmol GFP-h2NLS-L-TM in 8.3×10^6 cells, corresponding to a copy number of 13 000 copies of GFP-h2NLS-L-TM per cell. C) Similar as (A) but now for tcNLS-mCh and rgNLS-mCh co-expressed either with GFP-h2NLS-L-TM (1) or GFP-L-TM (2). The culture was grown to a density of 1.4×10^7 cells mL^{-1}. An equivalent of 7.2×10^6 cells was loaded on a SDS-PAA gel, together with a dilution series from 50 to 1600 fmol of purified mCh. D) Similar as (B) but now for tcNLS-mCh and rgNLS-mCh co-expressed either with GFP-h2NLS-L-TM or GFP-L-TM. We found 145 fmol tcNLS-mCh when co-expressed with GFP-h2NLS-L-TM and 169 fmol tcNLS-mCh when co-expressed with GFP-L-TM, corresponding to copy numbers of 12 000 and 15 000 per cell, respectively. We found 150 fmol rgNLS-mCh when co-expressed with GFP-h2NLS-L-TM and 198 fmol rgNLS-mCh when co-expressed with GFP-L-TM, corresponding to copy numbers of 13 000 and 17 000 per cell, respectively.

Figure S2: Image analysis to yield mean intensities at the NE of ER compartments. The NE/ER ratio describes the ratio of the mean fluorescence intensity at the NE over the mean fluorescence intensity at the ER. The NE/ER ratio thus estimates the relative concentrations of the reporter proteins at the NE and ER. The fluorescence intensity at the membranes is determined as described in (1) using the ZEN 2010B software (Zeiss), as follows: the region of interest, either the ER or the NE, is manually selected. In this example the region of interest (red lines) is selected to include the ER but not the NE. The pixel intensities in the region of interest are plotted in a histogram and visualized in the image. The selected in-focus membrane compartment is visible as a broad peak in the histogram, distinct from the out-of-focus or background fluorescence (upper panel). To determine the mean intensity of the in-focus fluorescence, the lower-threshold is manually set at the peak of the histogram (arrow). In the image is the ER shown as a more or less continuous system (II). The lower threshold is too low if out of focus signal is visible as a shade along the ER (I) or too high if interruptions are seen in the ER (III). By using threshold setting II (in the middle of I and III), we obtained reproducible results. Indicated below is the variation in mean intensity that results from variation in the settings of the lower threshold. In a double bind test we see an approximately 10% difference in eventual NE/ER ratio's.

Table S1: Membrane protein diffusion

Table S2: *S. cerevisiae* strains

Table S3: Plasmids

References

1. Powell L, Burke B. Internuclear exchange of an inner nuclear membrane protein (p55) in heterokaryons: in vivo evidence for the interaction of p55 with the nuclear lamina. J Cell Biol 1990;111:2225–2234.
2. Antonin W, Ungricht R, Kutay U. Traversing the NPC along the pore membrane: targeting of membrane proteins to the INM. Nucleus 2011;2:87–91.
3. Burns LT, Wente SR. Trafficking to uncharted territory of the nuclear envelope. Curr Opin Cell Biol 2012;24:341–349.
4. Lusk CP, Blobel G, King MC. Highway to the inner nuclear membrane: rules for the road. Nat Rev Mol Cell Biol 2007;8:414–420.
5. Zuleger N, Kerr AR, Schirmer EC. Many mechanisms, one entrance: membrane protein translocation into the nucleus. Cell Mol Life Sci 2012;69:2205–2216.
6. Meinema AC, Poolman B, Veenhoff LM. The transport of integral membrane proteins across the nuclear pore complex. Nucleus. 2012;3:322–329.
7. Worman HJ, Courvalin JC. The inner nuclear membrane. J Membr Biol 2000;177:1–11.
8. Soullam B, Worman HJ. Signals and structural features involved in integral membrane protein targeting to the inner nuclear membrane. J Cell Biol 1995;130:15–27.
9. Soullam B, Worman HJ. The amino-terminal domain of the lamin B receptor is a nuclear envelope targeting signal. J Cell Biol 1993;120:1093–1100.
10. Ellenberg J, Siggia ED, Moreira JE, Smith CL, Presley JF, Worman HJ, Lippincott-Schwartz J. Nuclear membrane dynamics and reassembly in living cells: targeting of an inner nuclear membrane protein in interphase and mitosis. J Cell Biol 1997;138:1193–1206.
11. Graumann K, Irons SL, Runions J, Evans DE. Retention and mobility of the mammalian lamin B receptor in the plant nuclear envelope. Biol Cell 2007;99:553–562.
12. Ostlund C, Ellenberg J, Hallberg E, Lippincott-Schwartz J, Worman HJ. Intracellular trafficking of emerin, the Emery-Dreifuss muscular dystrophy protein. J Cell Sci 1999;112:1709–1719.
13. Wu W, Lin F, Worman HJ. Intracellular trafficking of MAN1, an integral protein of the nuclear envelope inner membrane. J Cell Sci 2002;115:1361–1371.
14. Hinshaw JE, Carragher BO, Milligan RA. Architecture and design of the nuclear pore complex. Cell 1992;69:1133–1141.
15. Zuleger N, Korfali N, Schirmer EC. Inner nuclear membrane protein transport is mediated by multiple mechanisms. Biochem Soc Trans 2008;36:1373–1377.
16. King MC, Lusk CP, Blobel G. Karyopherin-mediated import of integral inner nuclear membrane proteins. Nature 2006;442:1003–1007.
17. Turgay Y, Ungricht R, Rothballer A, Kiss A, Csucs G, Horvath P, Kutay U. A classical NLS and the SUN domain contribute to the targeting of SUN2 to the inner nuclear membrane. EMBO J 2010;29:2262–2275.
18. Tapley EC, Ly N, Starr DA. Multiple mechanisms actively target the SUN protein UNC-84 to the inner nuclear membrane. Mol Biol Cell 2011;22:1739–1752.
19. Funakoshi T, Clever M, Watanabe A, Imamoto N. Localization of Pom121 to the inner nuclear membrane is required for an early step of interphase nuclear pore complex assembly. Mol Biol Cell 2011;22:1058–1069.
20. Meinema AC, Laba JK, Hapsari RA, Otten R, Mulder FA, Kralt A, van den Bogaart G, Lusk CP, Poolman B, Veenhoff LM. Long unfolded linkers facilitate membrane protein import through the nuclear pore complex. Science 2011;333:90–93.
21. Pemberton LF, Paschal BM. Mechanisms of receptor-mediated nuclear import and nuclear export. Traffic 2005;6:187–198.
22. Dingwall C, Laskey RA. Nuclear targeting sequences–a consensus? Trends Biochem Sci 1991;16:478–481.
23. Wente SR, Rout MP. The nuclear pore complex and nuclear transport. Cold Spring Harb Perspect Biol 2010;2:a000562.
24. Kahms M, Hüve J, Wesselmann R, Farr JC, Baumgärtel V, Peters R. Lighting up the nuclear pore complex. Eur J Cell Biol 2011;90:751–758.
25. Hahn S, Maurer P, Caesar S, Schlenstedt G. Classical NLS proteins from Saccharomyces cerevisiae. J Mol Biol 2008;379:678–694.
26. Lange A, McLane LM, Mills RE, Devine SE, Corbett AH. Expanding the definition of the classical bipartite nuclear localization signal. Traffic 2010;11:311–323.
27. Seedorf M, Damelin M, Kahana J, Taura T, Silver PA. Interactions between a nuclear transporter and a subset of nuclear pore complex proteins depend on Ran GTPase. Mol Cell Biol 1999;19:1547–1557.
28. Ghaemmaghami S, Huh WK, Bower K, Howson RW, Belle A, Dephoure N, O'Shea EK, Weissman JS. Global analysis of protein expression in yeast. Nature 2003;425:737–741.
29. Hahn S, Schlenstedt G. Importin beta-type nuclear transport receptors have distinct binding affinities for Ran-GTP. Biochem Biophys Res Commun 2011;406:383–388.
30. Lee DC, Aitchison JD. Kap104p-mediated nuclear import. Nuclear localization signals in mRNA-binding proteins and the role of Ran and Rna. J Biol Chem 1999;274:29031–29037.
31. Timney BL, Tetenbaum-Novatt J, Agate DS, Williams R, Zhang W, Chait BT, Rout MP. Simple kinetic relationships and nonspecific competition govern nuclear import rates in vivo. J Cell Biol 2006;175:579–593.
32. Haruki H, Nishikawa J, Laemmli UK. The anchor-away technique: rapid, conditional establishment of yeast mutant phenotypes. Mol Cell 2008;31:925–932.
33. Yewdell WT, Colombi P, Makhnevych T, Lusk CP. Lumenal interactions in nuclear pore complex assembly and stability. Mol Biol Cell 2011;22:1375–1388.
34. Nenninger A, Mastroianni G, Mullineaux CW. Size dependence of protein diffusion in the cytoplasm of Escherichia coli. J Bacteriol 2010;192:4535–4540.

35. Swaminathan R, Hoang CP, Verkman AS. Photobleaching recovery and anisotropy decay of green fluorescent protein GFP-S65T in solution and cells: cytoplasmic viscosity probed by green fluorescent protein translational and rotational diffusion. Biophys J 1997;72:1900–1907.
36. van den Bogaart G, Meinema AC, Krasnikov V, Veenhoff LM, Poolman B. Nuclear transport factor directs localization of protein synthesis during mitosis. Nat Cell Biol 2009;11:350–356.
37. Goodwin JS, Kenworthy AK. Photobleaching approaches to investigate diffusional mobility and trafficking of Ras in living cells. Methods 2005;37:154–164.
38. Schwoebel ED, Ho TH, Moore MS. The mechanism of inhibition of Ran-dependent nuclear transport by cellular ATP depletion. J Cell Biol 2002;157:963–974.
39. Shulga N, Roberts P, Gu Z, Spitz L, Tabb MM, Nomura M, Goldfarb DS. In vivo nuclear transport kinetics in Saccharomyces cerevisiae: a role for heat shock protein 70 during targeting and translocation. J Cell Biol 1996;135:329–339.
40. Görlich D, Pante N, Kutay U, Aebi U, Bischoff FR. Identification of different roles for RanGDP and RanGTP in nuclear protein import. EMBO J 1996;15:5584–5594.
41. Ribbeck K, Kutay U, Paraskeva E, Gorlich D. The translocation of transportin-cargo complexes through nuclear pores is independent of both Ran and energy. Curr Biol 1999;9:47–50.
42. Kutay U, Izaurralde E, Bischoff FR, Mattaj IW, Gorlich D. Dominant-negative mutants of importin-beta block multiple pathways of import and export through the nuclear pore complex. EMBO J 1997;16:1153–1163.
43. Deng M, Hochstrasser M. Spatially regulated ubiquitin ligation by an ER/nuclear membrane ligase. Nature 2006;443:827–831.
44. Nehls S, Snapp EL, Cole NB, Zaal KJ, Kenworthy AK, Roberts TH, Ellenberg J, Presley JF, Siggia E, Lippincott-Schwartz J. Dynamics and retention of misfolded proteins in native ER membranes. Nat Cell Biol 2000;2:288–295.
45. Zuleger N, Kelly DA, Richardson AC, Kerr AR, Goldberg MW, Goryachev AB, Schirmer EC. System analysis shows distinct mechanisms and common principles of nuclear envelope protein dynamics. J Cell Biol 2011;193:109–123.
46. West M, Zurek N, Hoenger A, Voeltz GK. A 3D analysis of yeast ER structure reveals how ER domains are organized by membrane curvature. J Cell Biol 2011;193:333–346.
47. Winey M, Yarar D, Giddings TH Jr, Mastronarde DN. Nuclear pore complex number and distribution throughout the Saccharomyces cerevisiae cell cycle by three-dimensional reconstruction from electron micrographs of nuclear envelopes. Mol Biol Cell 1997;8: 2119–2132.
48. Smith AE, Slepchenko BM, Schaff JC, Loew LM, Macara IG. Systems analysis of Ran transport. Science 2002;295:488–491.
49. Grund SE, Fischer T, Cabal GG, Antúnez O, Pérez-Ortín JE, Hurt E. The inner nuclear membrane protein Src1 associates with subtelomeric genes and alters their regulated gene expression. J Cell Biol 2008;182:897–910.
50. Mekhail K, Seebacher J, Gygi SP, Moazed D. Role for perinuclear chromosome tethering in maintenance of genome stability. Nature 2008;456:667–670.
51. Rodriguez-Navarro S, Igual JC, Perez-Ortin JE. SRC1: an intron-containing yeast gene involved in sister chromatid segregation. Yeast 2002;19:43–54.
52. Talamas JA, Hetzer MW. POM121 and Sun1 play a role in early steps of interphase NPC assembly. J Cell Biol 2011;194:27–37.
53. Yavuz S, Santarella-Mellwig R, Koch B, Jaedicke A, Mattaj IW, Antonin W. NLS-mediated NPC functions of the nucleoporin Pom121. FEBS Lett 2010;584:3292–3298.
54. Yang Q, Rout MP, Akey CW. Three-dimensional architecture of the isolated yeast nuclear pore complex: functional and evolutionary implications. Mol Cell 1998;1:223–234.
55. Frenkiel-Krispin D, Maco B, Aebi U, Medalia O. Structural analysis of a metazoan nuclear pore complex reveals a fused concentric ring architecture. J Mol Biol 2010;395:578–586.
56. Stoffler D, Feja B, Fahrenkrog B, Walz J, Typke D, Aebi U. Cryo-electron tomography provides novel insights into nuclear pore architecture: implications for nucleocytoplasmic transport. J Mol Biol 2003;328:119–130.
57. Akey CW, Radermacher M. Architecture of the Xenopus nuclear pore complex revealed by three-dimensional cryo-electron microscopy. J Cell Biol 1993;122:1–19.
58. Solmaz SR, Chauhan R, Blobel G, Melcak I. Molecular architecture of the transport channel of the nuclear pore complex. Cell 2011;147:590–602.
59. Galea CA, Nourse A, Wang Y, Sivakolundu SG, Heller WT, Kriwacki RW. Role of intrinsic flexibility in signal transduction mediated by the cell cycle regulator, p27 Kip1. J Mol Biol 2008;376:827–838.
60. Miyagi A, Tsunaka Y, Uchihashi T, Mayanagi K, Hirose S, Morikawa K, Ando T. Visualization of intrinsically disordered regions of proteins by high-speed atomic force microscopy. Chemphyschem 2008;9:1859–1866.
61. Brachmann CB, Davies A, Cost GJ, Caputo E, Li J, Hieter P, Boeke JD. Designer deletion strains derived from Saccharomyces cerevisiae S288C: a useful set of strains and plasmids for PCR-mediated gene disruption and other applications. Yeast 1998;14:115–132.
62. Huh WK, Falvo JV, Gerke LC, Carroll AS, Howson RW, Weissman JS, O'Shea EK. Global analysis of protein localization in budding yeast. Nature 2003;425:686–691.
63. Niedenthal RK, Riles L, Johnston M, Hegemann JH. Green fluorescent protein as a marker for gene expression and subcellular localization in budding yeast. Yeast 1996;12:773–786.
64. Schuck S, Prinz WA, Thorn KS, Voss C, Walter P. Membrane expansion alleviates endoplasmic reticulum stress independently of the unfolded protein response. J Cell Biol 2009;187:525–536.
65. Axelrod D, Koppel DE, Schlessinger J, Elson E, Webb WW. Mobility measurement by analysis of fluorescence photobleaching recovery kinetics. Biophys J 1976;16:1055–1069.
66. Tyson CB, Lord PG, Wheals AE. Dependency of size of Saccharomyces cerevisiae cells on growth rate. J Bacteriol 1979;138:92–98.
67. Prinz WA, Grzyb L, Veenhuis M, Kahana JA, Silver PA, Rapoport TA. Mutants affecting the structure of the cortical endoplasmic reticulum in Saccharomyces cerevisiae. J Cell Biol 2000;150:461–474.
68. Strambio-De-Castillia C, Blobel G, Rout MP. Isolation and characterization of nuclear envelopes from the yeast Saccharomyces. J Cell Biol 1995;131:19–31.